Journal of Applied Polymer Science

Nonlinear pyrolysis layer model for thermal behavior of nonhomogeneous charring materials

Weijie Li,[1] Haiming Huang,[1] Xiaoliang Xu,[2] Zhe Zhao[1]
[1]Institute of Engineering Mechanics, Beijing Jiaotong University, Beijing, 100044, China
[2]Beijing Institute of Near Space Vehicle's System Engineering, Beijing, 100076, China
Correspondence to: H. Huang (E-mail: huanghaiming@tsinghua.org.cn)

ABSTRACT: To improve the performance of charring materials as the thermal protection system in supersonic vehicles subjected to aerodynamic heating, we develop a nonlinear pyrolysis layer model of nonhomogeneous charring composites, propose a scheme of variable density in which the resin distribution of charring materials is taken as a piecewise linear function, and then simulate the thermal behavior of the design by means of the written calculation codes. This model reveals that the thermal behavior of charring materials depends not only upon several key parameters such as heat flux, moving interfaces, moving boundary and temperature-dependent thermal properties, but also upon variable density. Further numerical investigations point out that the pyrolysis layer plays a very important role in the thermal protection performance. This study will be useful for the optimization of the thermal protection system in supersonic vehicles. © 2015 Wiley Periodicals, Inc. J. Appl. Polym. Sci. **2015**, *132*, 42331.

KEYWORDS: composites; properties and characterization; theory and modeling; thermal properties

Received 10 December 2014; accepted 5 April 2015
DOI: 10.1002/app.42331

INTRODUCTION

The thermal behavior of gradient materials is an issue of growing interest like applying gradient materials in aerospace vehicles subjected to aerodynamic heat loads.[1] As is known to all, AVCOAT, which is charring materials of epoxy novolac resin with special additives in a fiberglass honeycomb, had been successfully applied in the thermal protection system (TPS) for Apollo vehicles. During the re-entry of a manned spacecraft, charring materials operate heavily by absorbing heat through pyrolysis and rejecting it via pyrolysis gas injection back into the boundary layer of gas.[2] Furthermore, oxygen in the boundary layer of gas field may get to the ablation surface and then some carbon on the surface at a high temperature is oxidized. The ablation surface gradually moves into inside the thermal protection layer.[3] Recently, many researchers have still focused on simulations for the thermal response of charring materials.[4–6] Lattimer *et al.*[7] measured the pyrolysis kinetic parameters and then analyzed in-depth temperature distribution by using the Arrhenius law. This method combines thermal analysis tests with the heat conduction equations, but the test results are highly dependent on the heating rate, which has significant difference with that of re-entry. Meanwhile, Li *et al.*[8] built the pyrolysis layer model of homogeneous materials. Thermal properties of charring ablators changing with pyrolysis were researched by both test and theoretical methods,[9–12] and the heat conduction equations with moving boundary or temperature-dependent thermal properties are strong nonlinear.[13–17] To make the thermal behavior calculation easier, Li *et al.*[18] regarded the pyrolysis layer as an interface. Regrettably, all models above are suitable only for homogeneous materials, not for nonhomogeneous materials. With the development of technology, nonhomogeneous composites will take the place of homogeneous ones in order to optimize the performance of TPS materials. Therefore, the mathematical model and the numerical method corresponding to the nonhomogeneous density composites have to be developed in the calculation for thermal behavior. In this study, we will present a scheme of variable density of AVCOAT and calculate the thermal behavior of nonhomogeneous composite by using the calculation codes written on the basis of the nonlinear pyrolysis layer model and the numerical method.

PYROLYSIS LAYER MODEL

Physical Model

The thermal response of charring materials under aerodynamic heating is as follows. First of all, charring materials can absorb heat by the heat capacity of materials themselves. When the surface temperature rises up to the beginning pyrolysis temperature T_{vp} of charring materials, the resin in surface materials starts to pyrolyze. Furthermore, when the surface materials are heated to the complete pyrolysis temperature T_{pc}, a char layer will form on the surface. Heating continues, the surface ablates and

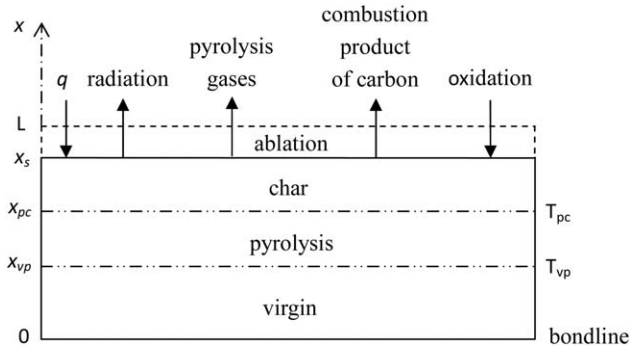

Figure 1. One-dimensional physical model.

gradually moves into the virgin layer after it reaches the ablation temperature T_s.

A one-dimensional physical model (Figure 1) can be established, since the temperature gradient vertically to the surface is much larger than those in the other orientations.[19,20]

In Figure 1, q is the heat flux, x_{vp}, x_{pc}, and x_s are, respectively, coordinates of two moving interfaces and one moving boundary, and L is the thickness of virgin materials without ablation. Along the x direction in space, the model is divided into four layers, namely the virgin layer, the pyrolysis layer, the char layer and the ablation layer. The physical-chemical phenomena of the four layers are the following:

a. The virgin layer: the zone where the temperature is lower than T_{vp}.
b. The pyrolysis layer: the zone where the temperature varies from T_{vp} to T_{pc}. It is just an unsteady and complex zone of ablator with two moving interfaces. On the one hand, materials pyrolyze and release mixed gases which mainly consist of methane, ethylene, acetylene and hydrogen. On the other hand, loose solid carbon is gradually forming. In this layer, there exists the seepage of pyrolysis gas, the chemical reactions between pyrolysis gas and solid carbon, and the changes in density. Further, mechanism of absorbing heat mainly depends on the pyrolysis and the heat capacities.
c. The char layer: the zone where the temperature is higher than T_{pc}, but lower than T_s. In this layer, there is a solid carbon structure through which the pyrolysis gases flow to the surface of the ablator. In addition, solid carbon and pyrolysis gases continue to absorb heat, and even the consequent cracking of pyrolysis gases is taken into consideration if necessary.
d. The ablation layer: the surface recession zone where the temperature is higher than T_s. It becomes a part of the boundary layer with both absorbing and releasing heat. In this layer, there is convection and radiation phenomenon with the oxidation reaction; what is more, ejecting pyrolysis gases and combustion products can change the velocity and temperature of gas flow.

Mathematical Model

A prediction mathematical model must be developed to calculate the thermal response of TPS during re-entry. The development of such a model involves a detailed consideration of each phenomenon in the above physical model and its relation to the over-all materials behavior. We put forward two basic assumptions to simplify the calculation. First, pyrolysis gases do not react chemically with the porous char layer through which it flows. Second, there is no secondary cracking of pyrolysis gases. Based on the two assumptions and the physical model, the one-dimensional process of heat and mass transfer in charring materials with variable density taken into account is described by the differential equations

$$\rho_1 c_1 \frac{\partial T(x,t)}{\partial t} = \frac{\partial}{\partial x}\left[k_1(\rho_1)\frac{\partial T(x,t)}{\partial x}\right] \quad 0 \le x < x_{vp} \tag{1}$$

$$\rho_2 c_2 \frac{\partial T(x,t)}{\partial t} = \frac{\partial}{\partial x}\left[k_2(\rho_2, T)\frac{\partial T(x,t)}{\partial x}\right] + \dot{m}_{g2} c_g \frac{\partial T(x,t)}{\partial x} + \frac{\partial \rho_2}{\partial t} \times h_g \quad x_{vp} \le x < x_{pc} \tag{2}$$

$$\rho_3 c_3 \frac{\partial T(x,t)}{\partial t} = \frac{\partial}{\partial x}\left[k_3(T)\frac{\partial T(x,t)}{\partial x}\right] + \dot{m}_{g3} c_g \frac{\partial T(x,t)}{\partial x} \quad x_{pc} \le x \le x_s \tag{3}$$

where ρ, c, and k are the density, the specific heat, and the thermal conductivity, respectively. $\dot{m}$is the mass injection flux per area, and h is the enthalpy. The subscripts 1, 2, 3, and g represent the virgin layer, the pyrolysis layer, the char layer and pyrolysis gas, respectively.

If the accumulation of gases is ignored, the mass injection flux per area yields to the change of density. The conservation of mass may be denoted by:

$$\frac{\partial \rho_2}{\partial t} = -\frac{d\dot{m}_{g2}}{dx} \tag{4}$$

$$\dot{m}_{g3} = \dot{m}_{g2}|_{x=x_c} \tag{5}$$

Noting that ρ_1 is a x-dependent function, k_1 depends on ρ_1, k_2 is a function of both ρ_2 and T, and k_3 is a temperature-dependent function, we can write

$$\frac{\partial}{\partial x}[k_1(\rho_1)] = \frac{dk_1}{d\rho_1}\frac{d\rho_1}{dx} \tag{6}$$

$$\frac{\partial}{\partial x}[k_2(\rho_2, T)] = \frac{\partial k_2}{\partial \rho_2}\frac{d\rho_2}{dT}\frac{\partial T}{\partial x} + \frac{\partial k_2}{\partial T}\frac{\partial T}{\partial x} \tag{7}$$

$$\frac{\partial}{\partial x}\left[k_3\frac{\partial T(x,t)}{\partial x}\right] = k_3\frac{\partial^2 T(x,t)}{\partial x^2} + \frac{dk_3}{dT}\left[\frac{\partial T(x,t)}{\partial x}\right]^2 \tag{8}$$

Introducing eqs. (6–8) into eqs. (1–3), we obtain

$$\rho_1 c_1 \frac{\partial T(x,t)}{\partial t} = k_1(\rho_1)\frac{\partial^2 T(x,t)}{\partial x^2} + \frac{dk_1}{ds_1}\frac{d\rho_1}{dx}\frac{\partial T(x,t)}{\partial x} \tag{9}$$

$$\left(\rho_2 c_2 - \frac{d\rho_2}{dT} \times h_g\right)\frac{\partial T(x,t)}{\partial t} = k_2\frac{\partial^2 T(x,t)}{\partial x^2} + \left[\frac{\partial k_2(\rho_2, T)}{\partial s_2}\frac{d\rho_2(T)}{dT} + \frac{\partial k_2(\rho_2, T)}{\partial T}\right]\left[\frac{\partial T(x,t)}{\partial x}\right]^2 + \dot{m}_{g2} c_g \frac{\partial T(x,t)}{\partial x} \tag{10}$$

$$\rho_3 c_3 \frac{\partial T(x,t)}{\partial t} = k_3\frac{\partial^2 T(x,t)}{\partial x^2} + \frac{dk_3}{dT}\left[\frac{\partial T(x,t)}{\partial x}\right]^2 + \dot{m}_{g3} c_g \frac{\partial T(x,t)}{\partial x} \tag{11}$$

It is evident that the nonlinear influence coming from the quadratic terms of eqs. (10) and (11) make the calculation difficult.

Suppose that the bondline of ablator is adiabatic, and the boundary conditions are expressed by the relations:

$$-k_1\frac{\partial T(x,t)}{\partial x}=0 \quad x=0 \tag{12}$$

$$T=\mathrm{T_p} \quad x=x_{vp} \tag{13}$$

$$T=\mathrm{T_c} \quad x=x_{pc} \tag{14}$$

$$-k_3\frac{\partial T(x,t)}{\partial x}=\varphi q-\varepsilon\sigma T_w^4+\dot{m}_{\mathrm{com}}h_{\mathrm{com}} \quad x=x_s \tag{15}$$

where subscript com and w represent the combustion of carbon and the ablation surface, respectively. ε is the emissivity of the ablation surface, σ is Stefan-Boltzmann constant, T_w is the surface temperature, the thermal blockage coefficient φ and the heat flux q are, respectively, defined by the relations.[21]

$$\varphi=1-0.58(\dot{m}_{g3}+\dot{m}_{\mathrm{com}})\frac{h_r}{q_{\mathrm{cold}}} \tag{16}$$

$$q=q_{\mathrm{cold}}\left(1-\frac{h_w}{h_r}\right) \tag{17}$$

in which $q_{\mathrm{cold}}$is cold-wall heat flux, the recovery enthalpy h_r is defined by the relation[22]

$$h_r=3\times10^{-5}q_{\mathrm{cold}}^2-146q_{\mathrm{cold}}+2\times10^8 \tag{18}$$

and the wall enthalpy h_w is:[21]

$$h_w=\begin{cases}8.33\times10^2T_w-2.49\times10^5, & 300K\le T_w<1500\mathrm{K}\\ -5\times10^3T_w+8.5\times10^6, & 1500K\le T_w<1700\mathrm{K}\\ 1.54\times10^3T_w-2.61\times10^6, & 1700K\le T_w\le3000\mathrm{K}\end{cases} \tag{19}$$

In terms of conservation of mass, mass injection flux per area of the surface carbon combustion is denoted by:

$$\dot{m}_{\mathrm{com}}=\rho_3\frac{\Delta x_s}{\Delta t} \tag{20}$$

where Δx_s is the moving boundary distance for each fixed time step Δt.

It is apparent that the heat flux at two moving interfaces must satisfy

$$-k_1\frac{\partial T(x,t)}{\partial x}=-k_2\frac{\partial T(x,t)}{\partial x} \quad x=x_{\mathrm{vp}} \tag{21}$$

$$-k_2\frac{\partial T(x,t)}{\partial x}=-k_3\frac{\partial T(x,t)}{\partial x} \quad x=x_{\mathrm{pc}} \tag{22}$$

In addition, an initial condition may be represented in the form

$$T(x)=T_0 \quad t=0 \tag{23}$$

It should be noted that the above mathematical model is strongly nonlinear with the temperature-dependent thermal properties, the moving interfaces and the moving boundary, which makes the calculation on the thermal behavior more difficult.

NUMERICAL APPROACHES

Discrete Format of the Transient Heat Conduction Equations

To calculate the above mathematical model, it is necessary to discretize the transient heat conduction eqs. (9–11). Here we adopt the central difference format in an implicit numerical method:

$$\frac{\partial T(x,t)}{\partial x}=\frac{T_{j+1}^n-T_{j-1}^n}{2\Delta x} \tag{24}$$

$$\frac{\partial T^2(x,t)}{\partial x^2}=\frac{T_{j+1}^n-2T_j^n+T_{j-1}^n}{(\Delta x)^2} \tag{25}$$

$$\frac{\partial T(x,t)}{\partial t}=\frac{T_j^n-T_j^{n-1}}{\Delta t} \tag{26}$$

introducing eq. (24) into the quadratic term in eq. (10) leads to the result

$$\left[\frac{\partial T(x,t)}{\partial x}\right]^2=\frac{\partial T(x,t)}{\partial x}\times\frac{\partial T(x,t)}{\partial x}=\frac{T_{j+1}^n-T_{j-1}^n}{2\Delta x}\times\frac{T_{j+1}^{n-1}-T_{j-1}^{n-1}}{2\Delta x} \tag{27}$$

By combining eqs. (24–27) with eq. (10) it is readily shown that

$$\frac{T_j^n-T_j^{n-1}}{\Delta t}=\frac{k_{2,j}^n}{\rho_{2,j}^nc_{2,j}^n-\frac{\rho_{2,j}^n-\rho_{2,j-1}^n}{T_j^n-T_{j-1}^n}\times h_g}\frac{T_{j+1}^n-2T_j^n+T_{j-1}^n}{(\Delta x)^2}+$$
$$\frac{\left[\frac{k_{2,j}^n-k_{2,j-1}^n}{\rho_{2,j}^n-\rho_{2,j-1}^n}\frac{\rho_{2,j}^n-\rho_{2,j-1}^n}{T_j^n-T_{j-1}^n}+\frac{k_{2,j}^n-k_{2,j-1}^n}{T_j^n-T_{j-1}^n}\right]\frac{T_{j+1}^{n-1}-T_{j-1}^{n-1}}{2\Delta x}+\dot{m}_{g2,j}^nc_g\frac{T_{j+1}^n-T_{j-1}^n}{2\Delta x}}{\rho_{2,j}^nc_{2,j}^n-\frac{\rho_{2,j}^n-\rho_{2,j-1}^n}{T_j^n-T_{j-1}^n}\times h_g} \tag{28}$$

where $\dot{m}_{g2j}^n$ is the mass injection flux per area of pyrolysis gas, which can be obtained by recursion formula as follows. Integration of eq. (4) with regard to x shows that

$$\dot{m}_{g2,j}^n=\int_{x_{vp}}^{x_j}\frac{\partial\rho_2}{\partial t}dx=\frac{d\rho_2}{dT}\int_{x_{vp}}^{x_j}\frac{\partial T}{\partial t}dx \tag{29}$$

$$\dot{m}_{g2,j+1}^n=\int_{x_{vp}}^{x_{j+1}}\frac{\partial\rho_2}{\partial t}dx=\frac{d\rho_2}{dT}\int_{x_{vp}}^{x_{j+1}}\frac{\partial T}{\partial t}dx \tag{30}$$

Using Newton-Cotes equation, introduction of eq. (30) into eq. (29) leads to the expression for the mass injection flux per area for j space step, namely,

$$m_{g2,j}^n=m_{g2,j+1}^n-\frac{\rho_{2,j}^n-\rho_{2,j-1}^n}{T_j^n-T_{j-1}^n}\cdot\frac{dx}{2}\cdot\left[\frac{k_{2,j}^n\frac{T_{j+1}^n-2T_j^n+T_{j-1}^n}{(\Delta x)^2}}{\rho_{2,j}^nc_{2,j}^n-\frac{\rho_{2,j}^n-\rho_{2,j-1}^n}{T_j^n-T_{j-1}^n}\times h_g}\right.$$
$$+\frac{k_{2,j+1}^n\frac{T_{j+2}^n-2T_{j+1}^n+T_j^n}{(\Delta x)^2}}{\rho_{2,j+1}^nc_{2,j+1}^n-\frac{\rho_{2,j}^n-\rho_{2,j-1}^n}{T_j^n-T_{j-1}^n}\times h_g}$$
$$+\frac{\left[\frac{k_{2,j}^n-k_{2,j-1}^n}{\rho_{2,j}^n-\rho_{2,j-1}^n}\frac{\rho_{2,j}^n-\rho_{2,j-1}^n}{T_j^n-T_{j-1}^n}+\frac{k_{2,j}^n-k_{2,j-1}^n}{T_j^n-T_{j-1}^n}\right]\left(\frac{T_{j+1}^n-T_{j-1}^n}{2\Delta x}\right)+m_{g2,j}^nc_g\frac{T_{j+1}^n-T_{j-1}^n}{2\Delta x}}{\rho_{2,j}^nc_{2,j}^n-\frac{\rho_{2,j}^n-\rho_{2,j-1}^n}{T_j^n-T_{j-1}^n}\times h_g}$$
$$\left.+\frac{\left[\frac{k_{2,j}^n-k_{2,j-1}^n}{\rho_{2,j}^n-\rho_{2,j-1}^n}\frac{\rho_{2,j}^n-\rho_{2,j-1}^n}{T_j^n-T_{j-1}^n}+\frac{k_{2,j}^n-k_{2,j-1}^n}{T_j^n-T_{j-1}^n}\right]\left(\frac{T_{j+2}^n-T_j^n}{2\Delta x}\right)+m_{g2,j+1}^nc_g\frac{T_{j+2}^n-T_j^n}{2\Delta x}}{\rho_{2,j+1}^nc_{2,j+1}^n-\frac{\rho_{2,j}^n-\rho_{2,j-1}^n}{T_j^n-T_{j-1}^n}\times h_g}\right] \tag{31}$$

Let

$$r_2=\frac{k^n_{2,j}}{\rho^n_{2,j}c^n_{2,j}-\frac{\rho^n_{2,j}-\rho^n_{2,j-1}}{T^n_j-T^n_{j-1}}\times h_g}\frac{\Delta t}{(\Delta x)^2},$$

$$z_2=\frac{\left(\frac{k^n_{2,j}-k^n_{2,j-1}}{\rho^n_{2,j}-\rho^n_{2,j-1}}\frac{\rho^n_{2,j}-\rho^n_{2,j-1}}{T^n_j-T^n_{j-1}}+\frac{k^n_{2,j}-k^n_{2,j-1}}{T^n_j-T^n_{j-1}}\right)\frac{T^{n-1}_{j+1}-T^{n-1}_{j-1}}{2\Delta x}+\dot{m}^n_{g2,j}c_g}{\rho^n_{2,j}c^n_{2,j}-\frac{\rho^n_{2,j}-\rho^n_{2,j-1}}{T^n_j-T^n_{j-1}}\times h_g}\frac{\Delta t}{2\Delta x},$$

and substituting r_2 and z_2 into eq. (28), we obtain

$$T^n_j-T^{n-1}_j=r_2(T^n_{j+1}-2T^n_j+T^n_{j-1})+z_2(T^n_{j+1}-T^n_{j-1}) \quad (32)$$

Similarly, eq. (32) is also taken as the discrete format of eqs. (9) and (11), but r and z corresponding to eqs. (9) and (11) are the following formulae, respectively:

$$r_1=\frac{k^n_{1,j}}{\rho^n_{1,j}c^n_{1,j}}\frac{\Delta t}{(\Delta x)^2}, \quad z_1=\frac{\frac{k^n_{1,j}-k^n_{1,j-1}}{\rho^n_{1,j}-\rho^n_{1,j-1}}\frac{\rho^n_{1,j}-\rho^n_{1,j-1}}{\Delta x}}{\rho^n_{1,j}c^n_{1,j}}\frac{\Delta t}{2\Delta x}$$

and

$$r_3=\frac{k^n_{3,j}}{s^n_{3,j}c^n_{3,j}}\frac{\Delta t}{(\Delta x)^2} \quad z_3=\frac{\frac{k^n_{3,j}-k^n_{3,j-1}}{T^n_j-T^n_{j-1}}\frac{T^{n-1}_{j+1}-T^{n-1}_{j-1}}{2\Delta x}+\dot{m}^n_{g3,j}c_g}{\rho^n_{3,j}c^n_{3,j}-\frac{\rho^n_{3,j}-\rho^n_{3,j-1}}{T^n_j-T^n_{j-1}}\times h_g}\frac{\Delta t}{2\Delta x}.$$

Determination of the Moving Boundary and the Moving Interfaces

It is the purpose of this discussion to show how moving distance Δx_s of boundary, moving distances Δx_{vp} and Δx_{pc} of interfaces for each time step can be calculated for the thermal behavior of ablator. By combining eqs. (20) and (24) with eq. (15) it is readily shown that

$$-k^n_{3,j}\frac{T^n_{j+1}-T^n_{j-1}}{2\Delta x_s}=\varphi q-\varepsilon\sigma T^4_w+\rho^n_{3,j}h_{com}\frac{\Delta x_s}{\Delta t} \quad x=x_s \quad (33)$$

where the temperature-dependent surface recession rate on the basis of reaction-rate-control regime,[12] for AVCOAT as an example, can be written in the following fitting function

$$\frac{\Delta x_s}{\Delta t}=\begin{cases}0, & 300\text{K}\le T_w<1200\text{K}\\ 1.1.76\times10^{-11}T_w^2-2.9124\times10^{-8}T_w+1.9179\times10^{-5}, & T_w\ge1200\text{K}\end{cases}$$

In view of the fact that the determination of the moving interfaces is very difficult, we have to introduce two functions representing the heat flux difference on both sides of moving interfaces $x=x_{vp}$ and $x=x_{pc}$, respectively:

$$F_{vp}(\Delta x_{vp},\Delta x_{pc})=\left\{-k_1\frac{\Delta T(x,t)}{\Delta x_{vp}}-\left[-k_2\frac{\Delta T(x,t)}{\Delta x_{vp}}\right]\right\}\Bigg|_{\begin{cases}x^{(t)}=x_{vp}{}^{(t-\Delta t)}-\Delta x_{vp}{}^{(t)}\\ x_{pc}{}^{(t)}=x_{pc}{}^{(t-\Delta t)}-\Delta x_{pc}{}^{(t)}\end{cases}}$$

$$F_{pc}(\Delta x_{vp},\Delta x_{pc})=\left\{-k_2\frac{\Delta T(x,t)}{\Delta x_{pc}}-\left[-k_3\frac{\Delta T(x,t)}{\Delta x_{pc}}\right]\right\}\Bigg|_{\begin{cases}x_{vp}{}^{(t)}=x_{vp}{}^{(t-\Delta t)}-\Delta x_{vp}{}^{(t)}\\ x^{(t)}=x_{pc}{}^{(t-\Delta t)}-\Delta x_{pc}{}^{(t)}\end{cases}}$$

It is apparent that the functions F_{vp} and F_{pc} depend on the in-depth temperature distribution and the moving interfaces. As Δx_{vp} and Δx_{pc} must meet the demand of eqs. (21) and (22), they can be determined by the matrix equation:

$$\begin{bmatrix}\frac{F_{vp}(\Delta x^{00}_{vp},\Delta x^0_{pc})-F_{vp}(\Delta x^0_{vp},\Delta x^0_{pc})}{\Delta x^{00}_{vp}-\Delta x^0_{vp}} & \frac{F_{vp}(\Delta x^0_{vp},\Delta x^{00}_{pc})-F_{vp}(\Delta x^0_{vp},\Delta x^0_{pc})}{\Delta x^{00}_{pc}-\Delta x^0_{pc}}\\ \frac{F_{pc}(\Delta x^{00}_{vp},\Delta x^0_{pc})-F_{pc}(\Delta x^0_{vp},\Delta x^0_{pc})}{\Delta x^{00}_{vp}-\Delta x^0_{vp}} & \frac{F_{pc}(\Delta x^0_{vp},\Delta x^{00}_{pc})-F_{pc}(\Delta x^0_{vp},\Delta x^0_{pc})}{\Delta x^{00}_{pc}-\Delta x^0_{pc}}\end{bmatrix}\times\begin{bmatrix}\Delta x_{vp}-\Delta x^{00}_{vp}\\ \Delta x_{pc}-\Delta x^{00}_{pc}\end{bmatrix}=\begin{bmatrix}F_{vp}(\Delta x^{00}_{vp},\Delta x^{00}_{pc})\\ F_{pc}(\Delta x^{00}_{vp},\Delta x^{00}_{pc})\end{bmatrix} \quad (34)$$

where Δx^0_{vp} and Δx^{00}_{vp} are assumed as different initial moving distances at the interface $x=x_{vp}$, as well as Δx^0_{pc} and Δx^{00}_{pc} are assumed as different initial moving distances at the interface $x=x_{pc}$ for each time step.

Furthermore, the steps involved in the Newton Secant method for obtaining Δx_{vp} and Δx_{pc} from eq. (34) are the following:

a. Suppose initial values of Δx^i_{vp} and Δx^i_{pc}, $(i=0, 00)$.
   Calculate the in-depth temperature distribution, using the discrete format of eqs. (9–11).

b. Calculate Δx_{vp} and Δx_{pc} using eq. (34). If $\left\|\begin{matrix}\Delta x_{vp}-\Delta x^{00}_{vp}\\ \Delta x_{pc}-\Delta x^{00}_{pc}\end{matrix}\right\|_\infty<\delta$, stop the iteration. δ is the permissible error. However, if $\left\|\begin{matrix}\Delta x_{vp}-\Delta x^{00}_{vp}\\ \Delta x_{pc}-\Delta x^{00}_{pc}\end{matrix}\right\|_\infty\ge\delta$, let $\Delta x^0_{vp}=\Delta x^{00}_{vp}$, $\Delta x^0_{pc}=\Delta x^{00}_{pc}$ and $\Delta x^{00}_{vp}=\Delta x_{vp}$, $\Delta x^{00}_{pc}=\Delta x_{pc}$, then return to step (b).

NUMERICAL EXAMPLE

In order to carry out numerical calculations it is convenient to write computer codes according to eqs. (32–34). Taking

Table I. Property Parameters as Constants

c_g (J kg^{-1} K^{-1})	ε	Σ (W m^{-2} K^{-4})	h_g (J/kg^3)	h_{com} (J/kg^3)	T_{vp} (K)	T_{pc} (K)
2093	0.65	5.6710^{-8}	8.7710^7	1.16310^7	589	811

AVCOAT as charring composites in this numerical example, we present a scheme of variable density of AVCOAT and calculate the thermal behavior of nonhomogeneous composite by means of the computer codes on the basis of MATLAB. In addition, thickness L is 37.5 mm.

Materials Properties

Property Parameters of the Virgin Layer and the Char Layer. Properties in the virgin layer and the char layer can be measured by experiments.[23,24] In these two layers, it is considered that some property parameters (e.g., enthalpy of pyrolysis and combustion of surface carbon, the specific heat of pyrolysis gas, the beginning pyrolysis temperature, the beginning carbonization temperature, the emissivity of ablation surface and Stefan-Boltzmann constant) are constants. The thermal conductivity in the virgin layer is a quadratic function of density similar to that of porous media in the references.[25–29]

$$k_1 = 1.42426\times10^{-7}\rho_1^2 \tag{35}$$

and the other parameters are functions of temperature,[24,25] which are listed in Tables (I–IV).

Property Parameters in the Pyrolysis Layer. Thermal properties in the pyrolysis layer are temperature-dependent. It is proved that dealing with the thermal properties between the virgin layer and the char layer with linear interpolation is reasonable in calculation.[24] Properties in the pyrolysis layer are illustrated by the relation

$$\rho_2 = \rho_1 - (\rho_1 - \rho_3)\times\left(\frac{T - T_{vp}}{T_{pc} - T_{vp}}\right) \quad \text{kg m}^{-3} \tag{36}$$

$$c_2 = c_1|_{x=x_{vp}} - (c_1|_{x=x_{vp}} - c_3|_{x=x_{pc}})\cdot\left(\frac{T - T_{vp}}{T_{pc} - T_{vp}}\right) \quad \text{J kg}^{-1}\text{K}^{-1} \tag{37}$$

$$k_2 = k_1|_{x=x_{vp}} - (k_1|_{x=x_{vp}} - k_3|_{x=x_{pc}})\times\left(\frac{T - T_{vp}}{T_{pc} - T_{vp}}\right) \quad \text{W m}^{-1}\text{K}^{-1} \tag{38}$$

Table II. Specific Heat of the Virgin Layer

Temperature (K)	Specific heat (J kg^{-1} K^{-1})
311	1457
367	1465
422	1549
478	1591
533	1758
589	1842

Boundary Conditions on the Surface

To perform the necessary trajectory simulations, we take Apollo 4 re-entry thermal environment (Figure 2)[23] as the boundary conditions on the surface, where the heat flux is a function of time and the total re-entry heating duration is ~550 s.

Nonhomogeneous Design

Owing to developments in the hypersonic vehicles, exacting standards are now demanded for thermal protection materials.[30] To optimize performance of TPS, let the density of resin changing with heat flux on the surface (i.e., when the heat flux becomes higher, the density of the materials increases. Otherwise, it decreases). The carbon distribution is uniform, and its density is 100 kg m^{-3}, while the resin distribution of charring materials is taken as a piecewise linear function in-depth density, which is

$$\rho_1 = \begin{cases} 300 & 0 \le x < \text{L}/2 \\ 2.13\times10^4 x - 300 & \text{L}/2 \le x < 3\text{L}/4 \\ -2.13\times10^4 x + 900 & 3\text{L}/4 \le x \le \text{L} \end{cases} \tag{39}$$

and is also shown in Figure 3.

Numerical Results

Based on the pyrolysis layer model and the numerical approaches, numerical experimentation in trajectory thermal behavior of the variable density AVCOAT composites under Apollo 4 re-entry environments is performed by means of the written codes. The over-all thermal response is as follows.

The bondline temperature of charring ablator is an important factor to evaluate charring materials property for that it is adjacent to the metal structure of vehicles. As seen in Figure 4, the bondline temperature keeps 300 K until 170 s, and then it rises gradually to 334 K from 170 to 550 s.

The tendency of the surface temperature history curve is similar to heat flux, shown in Figure 5. It rises abruptly before 80 s until reaching the first peak point 2782 K. Then it decreases to 1500 K before 200 s and keeps almost unchangeable until 350 s. After that, it rises again to another peak point 1912 K at 421 s. In the following heating time, it decreases from the second peak point to 1049 K. In order to identify the oscillation in the curve clearly in initial heating time, the local position is zoomed. The oscillation starts with the beginning of carbonization.

Thickness history of the char layer is shown in Figure 6. In the first 18 s, the char layer does not appear. Under the heat flux at the surface, it begins to increase rapidly from 18 to 150 s. The large gradient is caused by the great heat loads in this time period, which can be obtained by integration of heat flux in Figure 2. After that, it grows slowly till 450 s. In the final heating time, it keeps the horizon at 4.6 mm, because the heat flux in this period is small.

From Figure 7, we know that the pyrolysis layer is a thin layer. The thickness history curve of the pyrolysis layer is just an irregular curve. It rises rapidly from 0 to 0.4 mm in the first 25 s. The increase of curve is caused by that only the pyrolysis layer appears without forming any char layer. Then it goes down gradually until 50 s since the char layer begins increasing

Table III. Specific Heat of the Char Layer

Temperature (K)	Specific heat (J kg^{-1} K^{-1})
811	1549
1367	1725
2756	1725
3033	1926

abruptly. After 50 s, the thicknesses of both the char layer and the pyrolysis layer rise in different speeds. From 50 to 200 s, the thickness of the pyrolysis layer increases rapidly, while the thickness of the char layer rises smoothly, which leads the pyrolysis thickness increasing in this time period. From 200 to 450 s, the curve gradually rises and then decreases. The decreasing is due to the thickness of the char layer increasing. In following time, the curve keeps rising because that the char layer does not change in this time period.

The surface recession rate can be observed in Figure 8. It maintains zero before 33 s since that the surface recession does not appear. Then it rises suddenly to 80 s and gets the first peak point 0.29610 mm s^{-1} near the time point of the peak heat flux. After the peak point, it begins to decrease till 170 s then keeps the horizon. From 350 to 420s, the curve rises again to another peak point 0.004681 mm s^{-1}. In the following time, it decreases from 0.004681 to 0 mm s^{-1} till 500 s. Finally, no surface recession would appear since that the surface recession rate keeps at 0 mm s^{-1}. The oscillation in the curve near the first peak point is zoomed in this figure too.

Figure 9 shows the thickness histories of the surface recession for the design. In the first 33 s, the surface recession does not appear. Before initial heating time of 150 s, the surface recession thickness rises with a larger gradient. Then it rises a little in the flowing 250 s. At 400 s, a little larger gradient occurs. Finally, thickness keeps a plateau with the value 2.212 mm.

As shown in Figure 10, we can see the in-depth temperature distribution at 550 s. Firstly, the curve rises with a smooth concave curve from the bondline to 28.44 mm (the range of the virgin layer). We can see that the in-depth temperature of this stage rises extremely smoothly. Then the curve rises with a large gradient. The beginning of this stage is the temperature T_{vp}, and the end of this stage is the temperature T_{pc}. The curve of this stage has a range of 2.517 mm, which is the range of pyrolysis layer. From 30.957 to 35.288 mm, the curve rises with a large gradient convex curve. It is the stage of the char layer. The larger gradients of temperature distribution curve in the pyrolysis layer and the char layer are caused by that the thermal conductivities of these two layers are larger than that of the virgin

Table IV. Thermal Conductivity of the Char Layer

Temperature (K)	Thermal conductivity (W m^{-1} K^{-1})
922	0.242
1033	0.381
1256	0.614
1367	0.736
1589	0.935
1700	1.030
1922	1.212

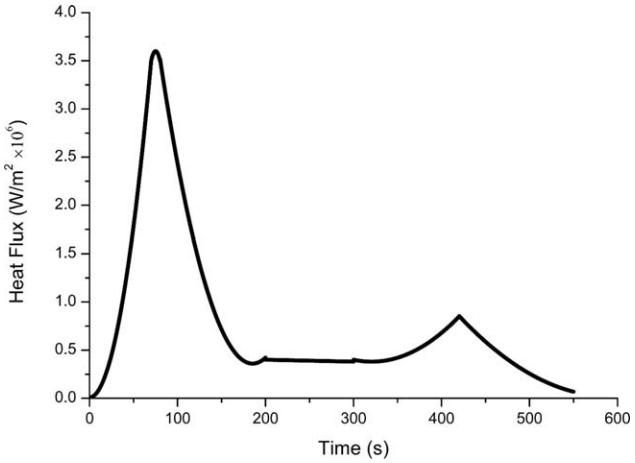

Figure 2. Cold-wall heat flux versus Time.

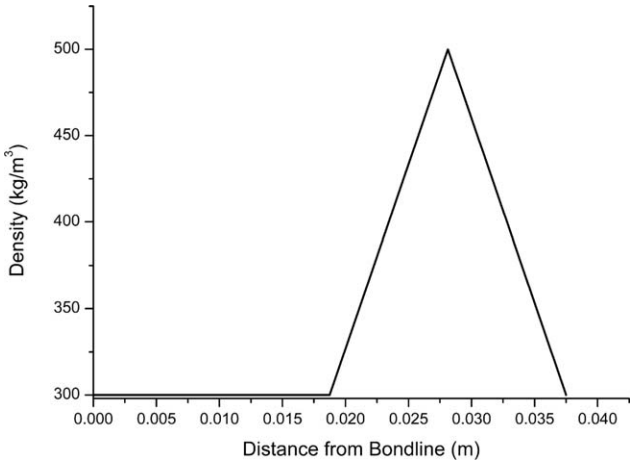

Figure 3. In-depth density distribution of resin.

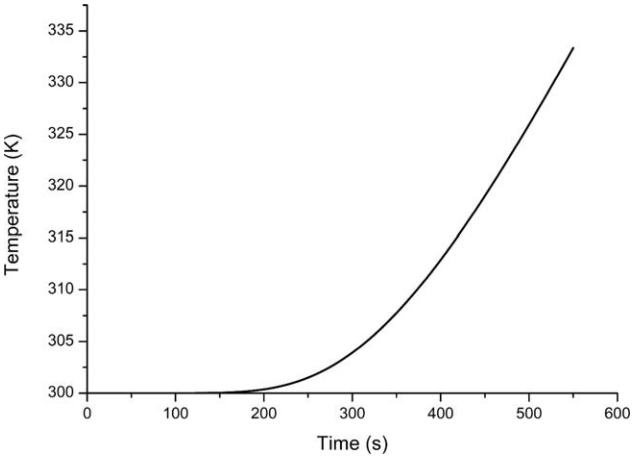

Figure 4. Bondline temperature history.

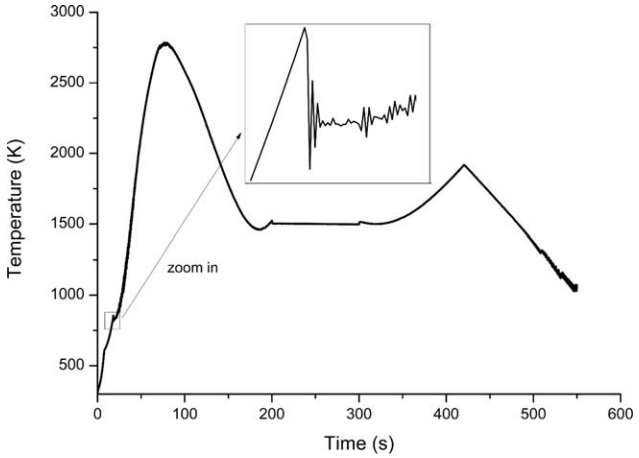

Figure 5. Surface temperature history.

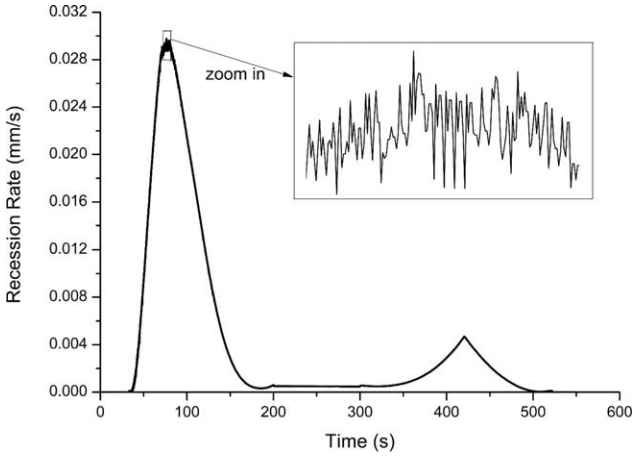

Figure 8. Surface recession rate histories.

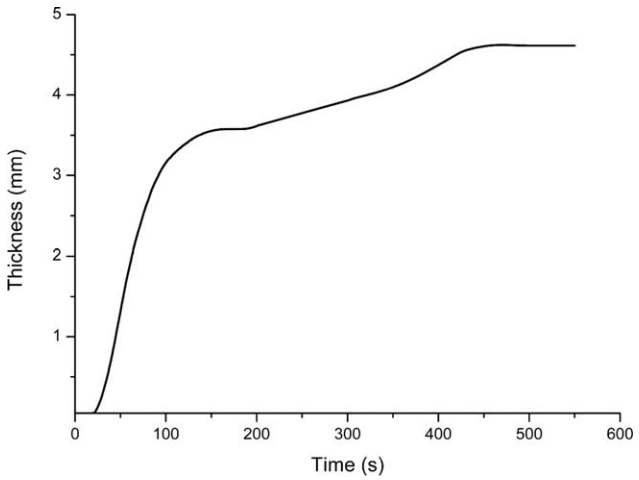

Figure 6. Thickness history of the char layer.

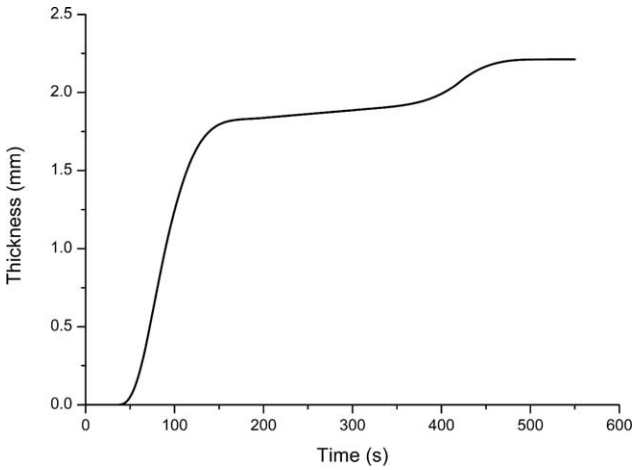

Figure 9. Surface recession histories.

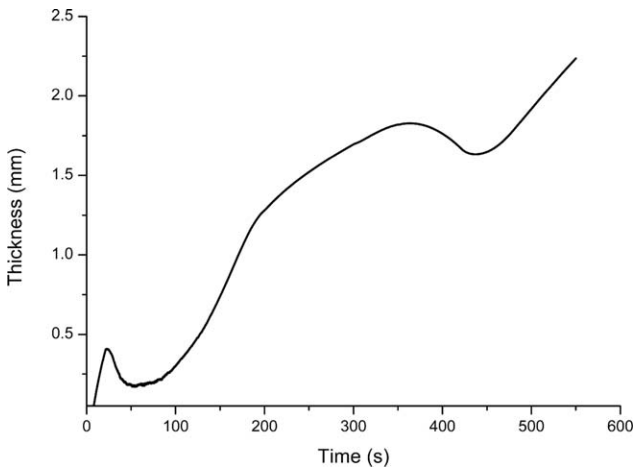

Figure 7. Thickness history of the pyrolysis layer.

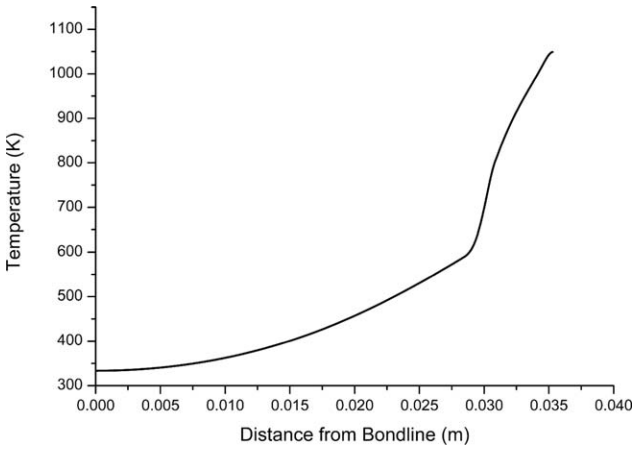

Figure 10. In-depth temperature distribution.

layer. In other words, the thermal conductivities increase gradually from 28.44 to 35.288 mm. The locations of the demarcation points of the curve are the interfaces of the three layers. From the Figure 10, it is obvious that the temperatures at the two moving boundaries are T_{vp} and T_{pc}, respectively. Additionally, subtracting the materials final thickness 35.288 mm from L leads the surface recession thickness 2.212 mm.

CONCLUSION

In this article, we propose a new approach for modeling the effect of density on the thermal behavior of charring ablator. The nonlinear pyrolysis layer model including pyrolysis and surface recession is developed for nonhomogeneous charring ablator. In our pyrolysis layer model, there are several key parameters: temperature-dependent thermal properties, variable density, moving interfaces and moving boundary. Note that nonlinear thermal behavior is directly relevant with these parameters. Introducing a piecewise linear density design, we have analyzed in detail the thermal behavior of the design by using the calculation codes written on the basis of the nonlinear pyrolysis layer model and the numerical approaches. From the numerical results, it can be concluded that the pyrolysis layer plays a very important role in the thermal protection performance. The use of this model will help us to improve TPS design for supersonic vehicles.

ACKNOWLEDGMENTS

The authors are grateful for support from the Project of Education Ministry of China (No. 62501036026) as well as the National Natural Sciences Foundation of China (Nos. 11472037 and 11272042).

NOMENCLATURE

ρ	Density (kg m^{-3})
c	Specific heat (J kg^{-1} K^{-1})
k	Thermal conductivity (W m^{-1} K^{-1})
$\dot{m}$	Mass injection flux per area (kg m^{-2} s^{-1})
h	Enthalpy (J kg^{-1})
q	Heat flux (W m^{-2})
ε	Emissivity of ablation surface
σ	Stefan-Boltzmann constant (W m^{-2} K^{-4})
T	Temperature (K)
L	Thickness of charring ablator (m)
x	Space coordinate (m)
t	Time (s)
F	Heat flux difference (W m^{-2})

Subscripts

1	Virgin
2	Pyrolysis layer
3	Char
vp	Interface between the virgin layer and the pyrolysis layer
pc	Interface between the pyrolysis layer and the char layer
s	Surface recession
g	Pyrolysis gas
cold	Cold wall
w	Ablation surface
r	Recovery
com	Combustion
i	Initial value of Newton Secant method for interface between the virgin layer and the pyrolysis layer

REFERENCES

1. Wang, B. L.; Mai, Y. W.; Zhang, X. H. *J. Am. Ceram. Soc.* **2005**, *88*, 683.
2. Chen, Y. K.; Milos, F. S.; Gokcen, T. *J. Spacecraft Rockets* **2010**, *47*, 775.
3. Suzuki, T.; Sakai, T.; Yamada, T. *J. Thermophys. Heat Tran.* **2007**, *21*, 257.
4. Stackpoole, M.; Thornton, J. ARC Report, 2010, ARC-E-DAA-TN2373.
5. Desai, T. G.; Lawson, J. W.; Keblinski, P. *Polymer* **2011**, *52*, 577.
6. Gibson, A. G.; Browne, T. N. A.; Feih, S. *J. Compos. Mater.* **2012**, *46*, 2005.
7. Lattimer, B. Y.; Ouellette, J.; Trelles, J. *Fire. Technol.* **2011**, *47*, 823.
8. Li, W. J.; Huang, H. M.; Ai, B. C.; Tian, Y. *Comput. Mater. Con.* **2014**, *43*, 175.
9. Mouritz, A. P.; Feih, S.; Kandare, E. *Part A Appl. Sci.* **2009**, *40*, 1800.
10. Panescu, D.; Whayne, J. G.; Fleischman, S. D. *IEEE Trans. Biomed. Eng.* **1995**, *42*, 879.
11. Park, J. M.; Kwon, D. J.; Wang, Z. J. *Compos. Part B Eng.* **2014**, *67*, 22.
12. Milos, F. S.; Scott, C. D.; Papa, S. V. D. *J. Spacecraft Rockets* **2014**, *51*, 397.
13. Johansson, B. T.; Lesnic, D.; Reeve, T. *Math. Comput. Simulat.* **2014**, *101*, 61.
14. Wang, G. L.; Zhao, G. Q.; Guan, Y. J. *J. Appl. Polym. Sci.* **2013**, *128*, 1339.
15. Hosseini, S. A.; Shahmorad, S.; Masoumi, H. *J. King Saud University Sci.* **2013**, *25*, 283.
16. Bhaskar, P. *J. Appl. Polym. Sci.* **2013**, *129*, 983.
17. Henderson, J. B.; Wiebelt, J. A.; Tant, M. R. *J. Compos. Mater.* **1985**, *19*, 579.
18. Li, W. J.; Huang, H. M.; Zhang, Z. M.; Xu, X. L. *Polym. Compos.* doi: 10.1002/pc.23263.
19. Belghazi, H.; Ganaoui, M.; Labbe, J. C. *Int. J. Therm. Sci.* **2010**, *49*, 311.
20. Huang, H. M.; Li, W. J.; Yu, H. L. *Therm. Sci.* **2014**, *18*, 1583.
21. Potts, R. L. *J. Spacecraft Rockets* **1995**, *32*, 200.
22. Swann, R. T.; Dow, M. B.; Tompkins, S. S. *J. Spacecraft* **1966**, *3*, 61.
23. Curry, D. M. NASA Report, 1965, NASA-TN-D-3150.
24. Williams, S. D.; Curry, D. M. NASA Report, 1992, NASA-RP-1289.
25. Abu-Hamdeh, N. H.; Khdair, A. I.; Reeder, R. C. *Int. J. Heat Mass Tran.* **2001**, *44*, 1073.
26. Narayanan, N.; Ramamurthy, K. *Cement Concrete Comp.* **2000**, *22*, 321.
27. Hrubesh, L. W.; Pekala, R. W. *J. Mater. Res.* **1994**, *9*, 731.
28. Woodside, W. *Can. J. Phys.* **1958**, *36*, 815.
29. Gupta, A.; Kneafsey, T. J.; Moridis, G. J. *J. Phys. Chem. B* **2006**, *110*, 16384.
30. Li, W. G.; Li, D. J.; Zhang, C. Z.; Fang, D. N. *Int. J. Fract.* **2012**, *176*, 181.